Published in final edited form as:
Science. 2014 August 22; 345(6199): 909–912. doi:10.1126/science.1251959.

Electron microscopy of gold nanoparticles at atomic resolution

Maia Azubel[1], **Jaakko Koivisto**[2], **Sami Malola**[3], **David Bushnell**[1], **Greg L. Hura**[4], **Ai Leen Koh**[5], **Hironori Tsunoyama**[6,#], **Tatsuya Tsukuda**[6,##], **Mika Pettersson**[2], **Hannu Häkkinen**[2,3], and **Roger D. Kornberg**[1,*]

[1]Department of Structural Biology, Stanford University School of Medicine, Stanford, CA 94305 [2]Department of Chemistry, Nanoscience Center, University of Jyväskylä, FI-40014 Jyväskylä, Finland [3]Department of Physics, Nanoscience Center, University of Jyväskylä, FI-40014 Jyväskylä, Finland [4]Physical Bioscience Division, Lawrence Berkeley National Lab, Berkeley CA, 94720 [5]Stanford Nanocharacterization Laboratory, Stanford University, Stanford, CA 94305 [6]Catalysis Research Center, Hokkaido University, Sapporo, Japan

Abstract

Structure determination of gold nanoparticles (AuNPs) is necessary for understanding their physical and chemical properties, and only one AuNP larger than 1 nm in diameter, an Au_{102}NP, has been solved to atomic resolution. Whereas the Au_{102}NP structure was determined by X-ray crystallography, other large AuNPs have proved refractory to this approach. Here we report the structure determination of an Au_{68}NP at atomic resolution by aberration-corrected transmission electron microscopy (AC-TEM), performed with the use of a minimal electron dose, an approach that should prove applicable to metal NPs in general. The structure of the Au_{68}NP was supported by small angle X-ray scattering (SAXS) and by comparison of observed infrared (IR) absorption spectra with calculations by density functional theory (DFT).

AuNPs are of both fundamental and practical interest. Particles on the order of a nanometer in diameter exhibit distinctive physical and chemical properties, with potential applications ranging from quantum electronics to biomedicine (1–3). The X-ray crystal structure of an Au_{102}NP, 1.5 nm in diameter, showed the cluster of gold atoms surrounded by 44 thiolate ligands (4). This atomic structure had three-fold significance: it identified the Au_{102}NP as a molecule, with a precise composition and unique arrangement of atoms; it led to the idea of the gold cluster as a “super-atom,” stabilized by the filling of electron shells; and it revealed a layer of alternating gold and ligand molecules at the interface with solution (5). Subsequent X-ray structures of much smaller organo-soluble AuNPs have supported the

*To whom correspondence should be addressed. kornberg@stanford.edu.
#Current address: Department of Chemistry, Faculty of Science and Technology, Keio University, Yokohama 223-8522, Japan
##Current address: Department of Chemistry, School of Science, The University of Tokyo, Tokyo 113-0033, Japan, Japan

Supplementary Materials
www.sciencemag.org
Materials and Methods
Figs. S1 – S11
References (28–32)
Coordinates files

super-atom idea, and have shown a similar gold-thiol surface layer (reviewed in Ref. (6)). Structure determination of other water-soluble AuNPs, and of larger NPs in general, has so far been unsuccessful. Although water-soluble AuNPs ranging from 1–3 nm have been crystallized, X-ray diffraction has not extended beyond about 5 Å resolution. Here we demonstrate the structure determination of a AuNP by a combination of a low-dose approach and AC-TEM, and report an atomic structure with both similarities and significant differences from the Au_{102}NP.

Whereas the thiolate ligand of the Au_{102}NP was *p*-mercaptobenzoic acid (*p*-MBA), we have now performed synthesis with *3*- mercaptobenzoic acid (*3*-MBA), resulting in a different set of uniform, water-soluble particles. The product of synthesis with a thiol:gold ratio of 2:1 formed a single sharp band upon gel electrophoresis, with a mobility greater than that of the Au_{102}NP, indicative of a smaller size, confirmed by cryo-TEM (Fig. S1). Electrospray-ionization (ESI) time-of-flight (TOF) mass spectrometry (MS) revealed four peaks corresponding to various charged forms of a compound of approximately 18 KDa with a gold core of approximately 14 KDa (Fig S2). A stable AuNP with a gold core of similar size was previously reported by Whetten and colleagues (7). Because the mass difference between 3 atoms of gold (m=591) and 4 molecules of 3-MBA (m=613) could not be resolved, the MS result was consistent with the possible molecular formulas $[Au_{71}(3\text{-MBA})_{27}]^{n-}$, $[Au_{68}(3\text{-MBA})_{31}]^{n-}$, $[Au_{68}(3\text{-MBA})_{32}]^{n-}$, $[Au_{65}(3\text{-MBA})_{35}]^{n-}$, and $[Au_{62}(3\text{-MBA})_{39}]^{n-}$. We could distinguish among these possibilities by thermogravimetric analysis (TGA) and X-ray photoelectron spectroscopy (XPS). TGA gave a weight loss of 24.4% (Fig. S3), compared with values of 26.2% expected for $Au_{68}(3\text{-MBA})_{31}$ or 26.8% expected for $Au_{68}(3\text{-MBA})_{32}$, both discrepancies within the error of the method (8). By contrast, expected TGA weight loss values of 29.6% for $Au_{65}(3\text{-MBA})_{35}$ and 33.0% for $Au_{62}(3\text{-MBA})_{39}$ represent discrepancies 3- to 5-fold greater. XPS gave signals corresponding to Au, S, C, and O (Fig. S4), and the peak intensities corresponding to Au_{4f} and S_{2p} were integrated to establish the ratio between Au and organic material. The difference between the values of 65.5% Au and 34.5% S measured and those of 68.7 % Au and 31.3 % S expected for $Au_{68}(3\text{-MBA})_{31}$ or 68.0% Au and 32.0% S expected for $Au_{68}(3\text{-MBA})_{32}$ were again within the error of the method (8). Values of 72.4% Au and 27.6% S expected for $Au_{71}(3\text{-MBA})_{27}$ were significantly different. Therefore, of the five molecular formulas consistent with the results from MS, all but two, $Au_{68}(3\text{-MBA})_{31}$ and $Au_{68}(3\text{-MBA})_{32}$, were ruled out by TGA and XPS.

The solubility of the Au_{68}NP and its stability in solution were remarkable. The Au_{68}NP could be derivatized with proteins and nucleic acids bearing exposed sulfhydryl groups (Fig. S5), and is therefore well suited for applications in biological science and biomedicine. The Au_{68}NP could be crystallized, forming hexagonal plates (Fig. S6), but X-ray diffraction did not extend beyond 5 Å resolution. Due to the apparent homogeneity of the Au_{68}NP, TEM and single particle reconstruction (9) could be pursued as an alternative for structure determination. Exposure to an electron dose normally used for data collection in materials science (thousands of $e^{-}/Å^2$) visibly perturbed the Au_{68} particles. We therefore turned to low dose procedures, routinely used for biological TEM, which reduce the exposure to the electron beam by orders of magnitude, by focusing on an area adjacent to that to be imaged

and then imaging for the minimal time required to record a signal above the noise, followed by improvement of the signal-to-noise ratio by image averaging. The low dose strategy was successful (Fig. 1a and Fig S7a): images of 939 particles acquired in this way and processed with the EMAN2 software package (10) (Fig S7), yielded an electron density map with 68 peaks (Fig. 1b and 1c). The peaks in the center of the map were of highest intensity, likely because they were most symmetrically arranged and most rigidly fixed. Identification of the peaks with gold atoms is justified, not only because their high intensities could be attributed only to heavy atoms, but by their number, by the distances between them, and by their packing. The distances ranged from 2.72–3.07 Å (Fig. 1d), in keeping with those for the gold core of the Au_{102}NP, which were from 2.8–3.1 Å (4). The packing was face-centered cubic (fcc) or truncated fcc-like, similar to that in a recently reported X-ray crystal structure of the organo-soluble $Au_{36}(SR)_{24}$ (11). The arrangement of the 68 gold atoms can be described as a 13-atom cuboctahedron with an atom in the center (Fig. 2a,b), surrounded by 24 atoms extending the fcc-like framework (Fig 2c), and additional 31 atoms deviating from fcc packing (Fig. 2d). A Fourier transform of a section of the electron density map (Fig. 1e) showed spots at 2.4 Å, consistent with this arrangement (atoms 2.7 – 3.0 Å apart with fcc packing have lattice planes with spacings of 2.3 – 2.55 Å), and demonstrating the resolution of the analysis.

Support for the EM structure came from SAXS, which gave a radius of gyration (Rg) of 7.6 Å, compared with an Rg calculated for the gold cluster of the EM structure of 5.72 Å. The larger measured Rg could be explained by aggregation of gold particles, which occurs in an ionic strength-dependent manner (12). The SAXS data could be fit by a mixture of monomer and dimer, with $Chi^2 = 1$ up to a reciprocal space distance (q value) of 0.44 $Å^{-1}$ (Fig. S8). At higher q values, a small discrepancy was observed, which may arise, in part, from the organic surface layer, neglected in the calculation of Rg from the EM structure. Indeed, the center-to-center distance of the dimer calculated from SAXS was 14 Å, consistent with a model of the surface layer (see below), whereas the diameter of the gold cluster from the EM structure, used in the calculation was 11.5 Å.

Sulfur atoms were introduced into the EM structure, with gold-sulfur distances of about 2.3 Å (Fig. 3a). Aside from 15 gold atoms fully coordinated with gold neighbors (the central atom, the 12 atoms on the vertices of the cuboctahedron, and another two atoms), all remaining gold atoms are available for Au-S bond formation. The final model, containing 32 atoms of S for consistency with the model from DFT described below, can be described as an Au_{15} fcc core decorated with 10 staple motifs (4, 6) and 12 V-shape (or bridge) motifs (13) (Fig 3a).

Additional support for the EM structure, came from DFT for the hypothetical compound $Au_{68}(SH)_{32}$. When a model of this compound, built from the coordinates of gold atoms in the EM structure, was relaxed to a local energy minimum with DFT, the positions of the gold atoms were largely unaffected (compare Figs. 2d and 2e). Most of the gold atoms were shifted by clearly less than 1 Å, with the exception of a few atoms in the surface layer (Fig. S9a). The positions of these atoms may be affected by hydrogen bonding between *3*-MBA ligands in the surface layer, as observed upon relaxation by DFT of the compound

$Au_{68}(SH)_{30}$(*3*-MBA)$_2$ (Fig. S9b). The DFT model displayed gold-sulfur motifs (Fig. 3b) similar to those produced by manual building of sulfur atoms into the EM structure (Fig. 3a).

The electronic structure of the Au_{68}NP was investigated by IR and UV-vis spectroscopy and linear-response, time-dependent DFT calculations (LR-TDDFT). The IR-spectrum showed discrete absorption peaks at approximately 4200 cm^{-1} (0.52 eV) and 5250 cm^{-1} (0.65 eV) and a split transition at 6100 cm^{-1} (0.76 eV) (Fig. 4). A fourth peak at 2500 cm^{-1} (0.31 eV) could not be assigned to any known vibrational mode. This peak persisted even after removing the vibrational contribution of the ligand layer (Fig S10), so we attributed the peak to an electronic transition. The optical gap of the Au_{68}NP is therefore at 2500 cm^{-1} (0.31 eV), which is significantly lower than the gap of 0.45 eV observed for the larger Au_{102}(*p*-MBA)$_{44}$ cluster (14). This result is in contrast with the trend towards smaller optical gap with increasing cluster size, reported for clusters of 25–144 gold atoms (15–20), and expected to approach zero for bulk metal. The optical gap of the Au_{68}NP is presumably lower because of deviation from spherical symmetry, so the cluster wave functions cannot follow a spherical form as they do in the case of Au_{102}NP. The spectrum of the DFT-relaxed $Au_{68}(SH)_{32}$ cluster obtained from the LR-TDDFT calculations (Fig. 4) reproduces the experimental spectral features (positions of absorption lines, not line shapes, which depend on the smoothing function applied in the calculations) with remarkable accuracy. Intensities are in good agreement for all but the first two transitions. In the UV-vis range, both the measured and computational spectra are rather featureless. This is in contrast with the spectra of the smaller organo-soluble $Au_{25}(SCH_2CH_2Ph)_{18}$ and $Au_{38}(SCH_2CH_2Ph)_{24}$ NPs that show significant absorption features in the UV-vis range (15–19). Additional LR-TDDFT calculations of possible compounds in the range of $Au_{68}(SR)_{31–34}$ (including $Au_{68}(SR)_{32}$ but with different arrangements of gold atoms) did not reproduce the measured IR data in the optical gap region satisfactorily (Fig. S11).

The notable findings of this work are three-fold: (i) the synthesis of a water-soluble AuNP, homogeneous in size, remarkably stable in solution, and nevertheless reactive towards sulfhydryl compounds, including proteins, (ii) the successful determination of atomic structure by EM, not previously reported, and (iii) the difference between the structure obtained and the only other structure of a large, water-soluble particle, the Au_{102}NP, solved by X-ray diffraction.

The atomic structure of the Au_{68}NP differs from that of the Au_{102}NP, in two important aspects. The symmetry of the Au_{68}NP is lower, and the electronic structure does not indicate a filled electronic shell (5). Whereas the Au_{102}NP exhibits global symmetry, based on a truncated decahedral core, with all remaining atoms following fcc packing rules, the Au_{68}NP is based almost entirely on local fcc packing. The low-symmetry Au_{68}NP structure differs from a proposal from theory for a metal core of higher symmetry for an organo-soluble particle of similar size, [$Au_{67}(SR)_{35}$] (21).

Structure determination of water-soluble AuNPs by EM is important because although many can be crystallized, only Au_{102}NP crystals so far diffract to atomic resolution. Aberration-corrected transmission electron microscopes are capable of revealing individual heavy atoms (22). Structures of large metal particles imaged under high dose conditions have been

reported: the results of model-fitting to EM data (23, 24); actual reconstructions from electron micrographs, in which the exact positions of individual atoms were not fully resolved (25); and results for bulk-like solid state systems where atoms are arranged in columns (26, 27). Our implementation of low dose techniques from biological TEM, combined with the power of the aberration-corrected transmission microscope, has revealed the atomic structure of an AuNP without any prior knowledge, model-fitting, or assumptions about packing, and should be generally applicable. The way is open to the structure determination many more metal nanoparticles and discovery of the general principles of nanoparticle organization.

Supplementary Material

Refer to Web version on PubMed Central for supplementary material.

Acknowledgments

The work at Stanford was supported by the HFSPO (M.A.) and by NIH AI-21144 (R.D.K). The work at the University of Jyväskylä was supported by the Academy of Finland (H.H. and M.P.) and the national graduate school in computational chemistry and spectroscopy LASKEMO (J.K.). G.L.H efforts supported by DOE BER grant No. DE-AC02-05CH11231 under Integrated Analysis Technologies (IDAT). Phil Robinson is thanked for assistance with EM processing and helpful discussions. Eero Hulkko and P. Andre Clayborne are thanked for help with spectroscopic experiments and preliminary computations, respectively.

References and Notes

1. Rosi NL, Giljohann DA, Thaxton CS, Lytton-Jean AKR, Han MS, Mirkin CA. Oligonucleotide-Modified Gold Nanoparticles for Intracellular Gene Regulation. Science. 2006; 312:1027–1030. published online EpubMay 19, 2006. 10.1126/science.1125559 [PubMed: 16709779]
2. Qian X, Peng XH, Ansari DO, Yin-Goen Q, Chen GZ, Shin DM, Yang L, Young AN, Wang MD, Nie S. In vivo tumor targeting and spectroscopic detection with surface-enhanced Raman nanoparticle tags. Nat Biotech. 2008; 26:83–90.
3. Daniel M-C, Astruc D. Gold Nanoparticles: Assembly, Supramolecular Chemistry, Quantum-Size-Related Properties, and Applications toward Biology, Catalysis, and Nanotechnology. Chemical Reviews. 2003; 104:293–346. published online Epub2004/01/01. 10.1021/cr030698+ [PubMed: 14719978]
4. Jadzinsky PD, Calero G, Ackerson CJ, Bushnell DA, Kornberg RD. Structure of a Thiol Monolayer-Protected Gold Nanoparticle at 1.1 √Ö Resolution. Science. 2007; 318:430–433. published online EpubOctober 19, 2007. 10.1126/science.1148624 [PubMed: 17947577]
5. Walter M, Akola J, Lopez-Acevedo O, Jadzinsky PD, Calero G, Ackerson CJ, Whetten RL, Grönbeck H, Häkkinen H. A unified view of ligand-protected gold clusters as superatom complexes. Proceedings of the National Academy of Sciences. 2008; 105:9157–9162. published online EpubJuly 8, 2008. 10.1073/pnas.0801001105
6. Häkkinen H. The gold-sulfur interface at the nanoscale. Nature Chemistry. 2012; 4:443–455.10.1038/nchem.1352
7. Whetten RL, Khoury JT, Alvarez MM, Murthy S, Vezmar I, Wang ZL, Stephens PW, Cleveland CL, Luedtke WD, Landman U. Nanocrystal gold molecules. Advanced Materials. 1996; 8:428–433.10.1002/adma.19960080513
8. Levi-Kalisman Y, Jadzinsky PD, Kalisman N, Tsunoyama H, Tsukuda T, Bushnell DA, Kornberg RD. Synthesis and Characterization of Au102(p-MBA)44 Nanoparticles. Journal of the American Chemical Society. 2011; 133:2976–2982. published online Epub2013/11/05. 10.1021/ja109131w [PubMed: 21319754]

9. Frank J. SINGLE-PARTICLE IMAGING OF MACROMOLECULES BY CRYO-ELECTRON MICROSCOPY. Annual Review of Biophysics and Biomolecular Structure. 2002; 31:303–319.10.1146/annurev.biophys.31.082901.134202
10. Tang G, Peng L, Baldwin PR, Mann DS, Jiang W, Rees I, Ludtke SJ. EMAN2: An extensible image processing suite for electron microscopy. Journal of Structural Biology. 2007; 157:38–46. http://dx.doi.org/10.1016/j.jsb.2006.05.009. [PubMed: 16859925]
11. Zeng C, Qian H, Li T, Li G, Rosi NL, Yoon B, Barnett RN, Whetten RL, Landman U, Jin R. Total Structure and Electronic Properties of the Gold Nanocrystal Au36(SR)24. Angewandte Chemie International Edition. 2012; 51:13114–13118.10.1002/anie.201207098
12. See supplementary materials on Science Online.
13. Häkkinen H, Walter M, Grönbeck H. Divide and Protect: Capping Gold Nanoclusters with Molecular Gold−Thiolate Rings. The Journal of Physical Chemistry B. 2006; 110:9927–9931. published online Epub2006/05/01. 10.1021/jp0619787 [PubMed: 16706449]
14. Hulkko E, Lopez-Acevedo O, Koivisto J, Levi-Kalisman Y, Kornberg RD, Pettersson M, Häkkinen H. Electronic and Vibrational Signatures of the Au102(p-MBA)44 Cluster. Journal of the American Chemical Society. 2011; 133:3752–3755. published online Epub2011/03/23. 10.1021/ja111077e [PubMed: 21348523]
15. Akola J, Walter M, Whetten RL, Häkkinen H, Grönbeck H. On the Structure of Thiolate-Protected Au25. Journal of the American Chemical Society. 2008; 130:3756–3757. published online Epub2008/03/01. 10.1021/ja800594p [PubMed: 18321117]
16. Heaven MW, Dass A, White PS, Holt KM, Murray RW. Crystal Structure of the Gold Nanoparticle [N(C8H17)4][Au25(SCH2CH2Ph)18]. Journal of the American Chemical Society. 2008; 130:3754–3755. published online Epub2013/11/04. 10.1021/ja800561b [PubMed: 18321116]
17. Zhu M, Aikens CM, Hollander FJ, Schatz GC, Jin R. Correlating the Crystal Structure of A Thiol-Protected Au25 Cluster and Optical Properties. Journal of the American Chemical Society. 2008; 130:5883–5885. published online Epub2013/11/04. 10.1021/ja801173r [PubMed: 18407639]
18. Lopez-Acevedo O, Tsunoyama H, Tsukuda T, Häkkinen H, Aikens CM. Chirality and Electronic Structure of the Thiolate-Protected Au38 Nanocluster. Journal of the American Chemical Society. 2010; 132:8210–8218. published online Epub2010/06/16. 10.1021/ja102934q [PubMed: 20499877]
19. Qian H, Eckenhoff WT, Zhu Y, Pintauer T, Jin R. Total Structure Determination of Thiolate-Protected Au38 Nanoparticles. Journal of the American Chemical Society. 2010; 132:8280–8281. published online Epub2010/06/23. 10.1021/ja103592z [PubMed: 20515047]
20. Koivisto J, Salorinne K, Mustalahti S, Lahtinen T, Malola S, Häkkinen H, Pettersson M. Vibrational Perturbations and Ligand–Layer Coupling in a Single Crystal of Au144(SC2H4Ph)60 Nanocluster. The Journal of Physical Chemistry Letters. 2014; 5:387–392. published online Epub2014/01/16. 10.1021/jz4026003
21. Nimmala PR, Yoon B, Whetten RL, Landman U, Dass A. Au67(SR)35 Nanomolecules: Characteristic Size-Specific Optical, Electrochemical, Structural Properties and First-Principles Theoretical Analysis. The Journal of Physical Chemistry A. 2013; 117:504–517. published online Epub2013/01/17. 10.1021/jp311491v [PubMed: 23289925]
22. Scholl JA, Koh AL, Dionne JA. Quantum plasmon resonances of individual metallic nanoparticles. Nature. 2012; 483:421–427. [PubMed: 22437611]
23. Bahena D, Bhattarai N, Santiago U, Tlahuice A, Ponce A, Bach SBH, Yoon B, Whetten RL, Landman U, Jose-Yacaman M. STEM Electron Diffraction and High-Resolution Images Used in the Determination of the Crystal Structure of the Au144(SR)60 Cluster. The Journal of Physical Chemistry Letters. 4:975–981. published online Epub2013/11/05. 10.1021/jz400111d [PubMed: 23687562]
24. Li ZY, Young NP, Di Vece M, Palomba S, Palmer RE, Bleloch AL, Curley BC, Johnston RL, Jiang J, Yuan J. Three-dimensional atomic-scale structure of size-selected gold nanoclusters. Nature. 2008; 451:46–48. [PubMed: 18066049]

25. Scott MC, Chen CC, Mecklenburg M, Zhu C, Xu R, Ercius P, Dahmen U, Regan BC, Miao J. Electron tomography at 2.4-angstrom resolution. Nature. 2012; 483:444–447. [PubMed: 22437612]
26. Van Aert S, Batenburg KJ, Rossell MD, Erni R, Van Tendeloo G. Three-dimensional atomic imaging of crystalline nanoparticles. Nature. 2011; 470:374–377. published online Epub02/17/print http://www.nature.com/nature/journal/v470/n7334/abs/10.1038-nature09741-unlocked.html#supplementary-information. [PubMed: 21289625]
27. Goris B, Bals S, Van den Broek W, Carbó-Argibay E, Gómez-Graña S, Liz-Marzán LM, Van Tendeloo G. Atomic-scale determination of surface facets in gold nanorods. Nat Mater. 2012; 11:930–935. published online Epub11//print http://www.nature.com/nmat/journal/v11/n11/abs/nmat3462.html#supplementary-information. [PubMed: 23085569]
28. Negishi Y, Nobusada K, Tsukuda T. Glutathione-Protected Gold Clusters Revisited:, Äâ Bridging the Gap between Gold(I), àíThiolate Complexes and Thiolate-Protected Gold Nanocrystals. Journal of the American Chemical Society. 2005; 127:5261–5270. published online Epub2013/11/11. 10.1021/ja042218h [PubMed: 15810862]
29. Winn MD, Ballard CC, Cowtan KD, Dodson EJ, Emsley P, Evans PR, Keegan RM, Krissinel EB, Leslie AGW, McCoy A, McNicholas SJ, Murshudov GN, Pannu NS, Potterton EA, Powell HR, Read RJ, Vagin A, Wilson KS. Overview of the CCP4 suite and current developments. Acta Crystallographica Section D. 2011; 67:235–242.10.1107/S0907444910045749
30. Hura GL, Menon AL, Hammel M, Rambo RP, Poole FL Ii, Tsutakawa SE, Jenney FE Jr, Classen S, Frankel KA, Hopkins RC, Yang S-j, Scott JW, Dillard BD, Adams MWW, Tainer JA. Robust, high-throughput solution structural analyses by small angle X-ray scattering (SAXS). Nat Meth. 2009; 6:606–612.
31. Enkovaara J, Rostgaard C, Mortensen JJ, Chen J, Dułak M, Ferrighi L, Gavnholt J, Glinsvad C, Haikola V, Hansen HA, Kristoffersen HH, Kuisma M, Larsen AH, Lehtovaara L, Ljungberg M, Lopez-Acevedo O, Moses PG, Ojanen J, Olsen T, Petzold V, Romero NA, Stausholm-Møller J, Strange M, Tritsaris GA, Vanin M, Walter M, Hammer B, Häkkinen H, Madsen GKH, Nieminen RM, Nørskov JK, Puska M, Rantala TT, Schiøtz J, Thygesen KS, Jacobsen KW. Electronic structure calculations with GPAW: a real-space implementation of the projector augmented-wave method. Journal of Physics: Condensed Matter. 2010; 22:253202.
32. Walter M, Häkkinen H, Lehtovaara L, Puska M, Enkovaara J, Rostgaard C, Mortensen JJ. Time-dependent density-functional theory in the projector augmented-wave method. The Journal of Chemical Physics. 2008; 128:244101. http://dx.doi.org/10.1063/1.2943138. [PubMed: 18601311]

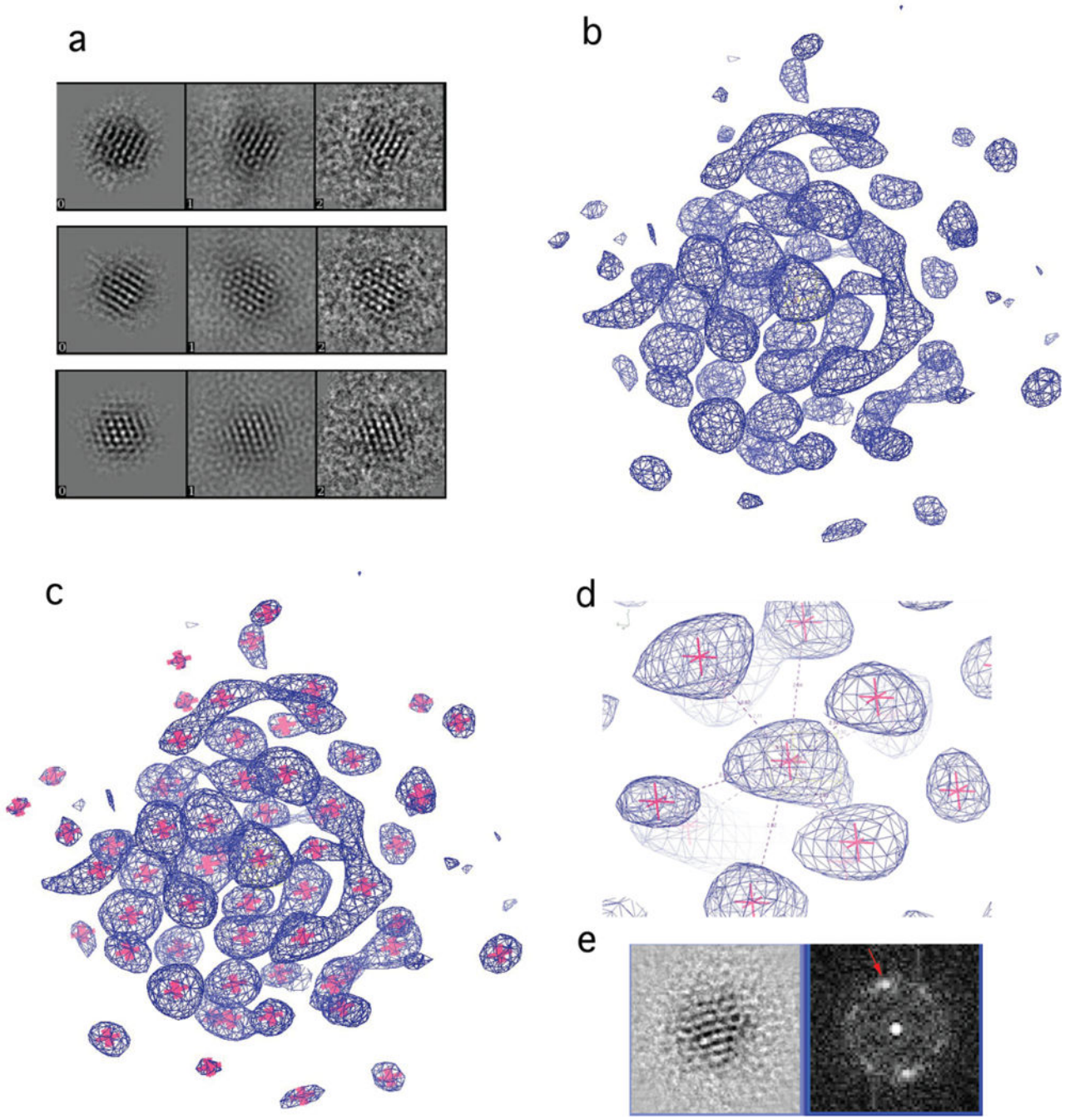

Figure 1. Three-dimensional reconstruction of Au_{68}NP structure from electron micrographs

(a) Representative components of the reconstruction. Left panel, a back projection from the reconstruction; middle panel, a corresponding class average of the EM images; right panel, EM images. (b–d) Electron density map, blue mesh. Pink stars (c–d) show the position of atomic coordinates for gold atoms. (d) Region of the electron density map surrounding the central atom. Dashed lines show coordination of the central atom; numbers indicate gold-gold distances in Å. (e) A cross-section of the 3D reconstruction (left panel) and its Fourier transform (right panel). Red arrow indicates spots at 2.4Å resolution.

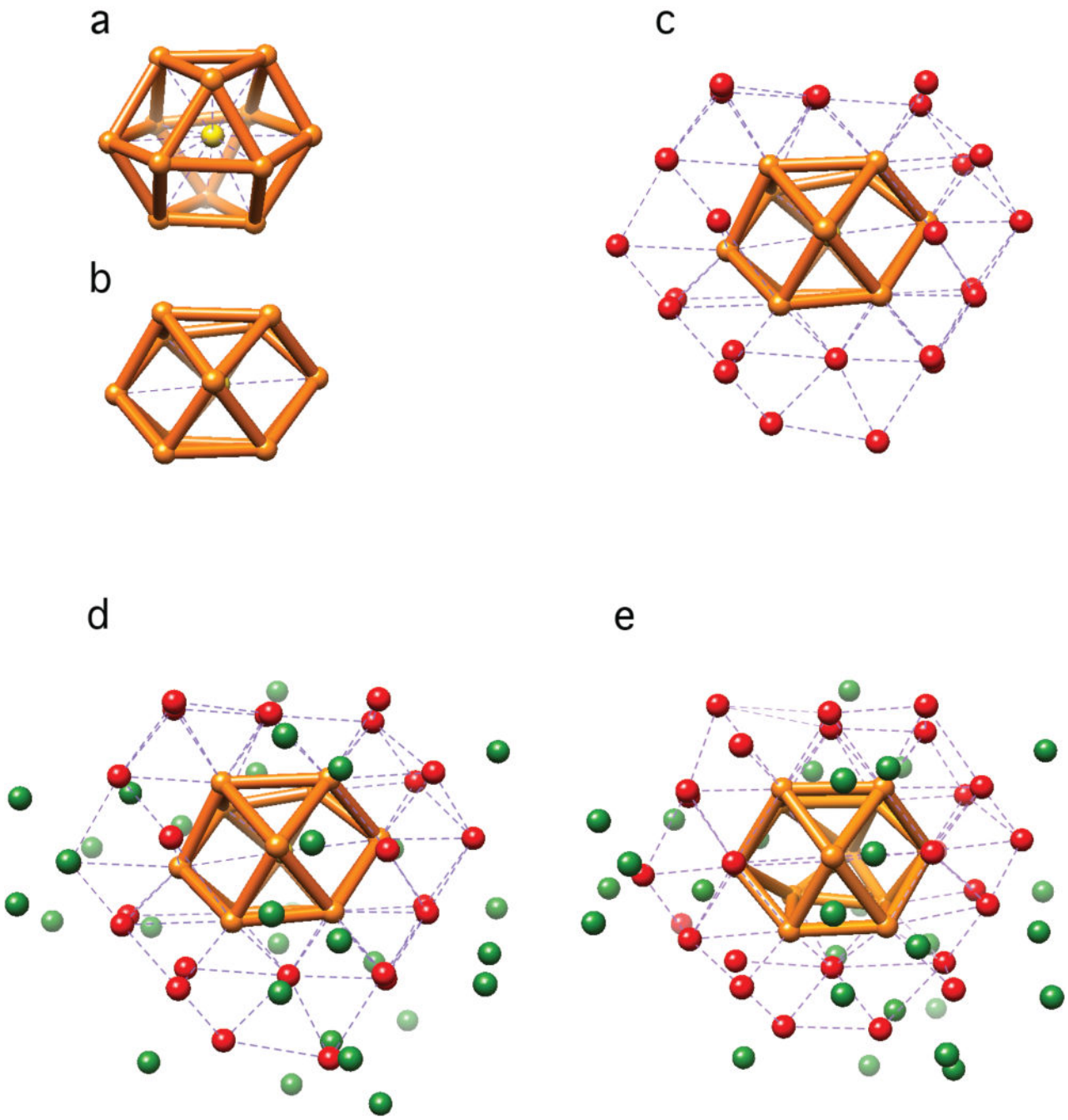

Figure 2. Arrangement of gold atoms in Au_{68}NP

(a–d) Coordinates. (a,b) Two orthogonal views of the central 13 atoms: central atom (yellow) caged in a cuboctahedron (orange). (c) Additional 24 atoms (red) extending the fcc-like framework. (d) All 68 atoms. In green are atoms with lower or no apparent symmetry. (e) Au_{68} model from DFT.

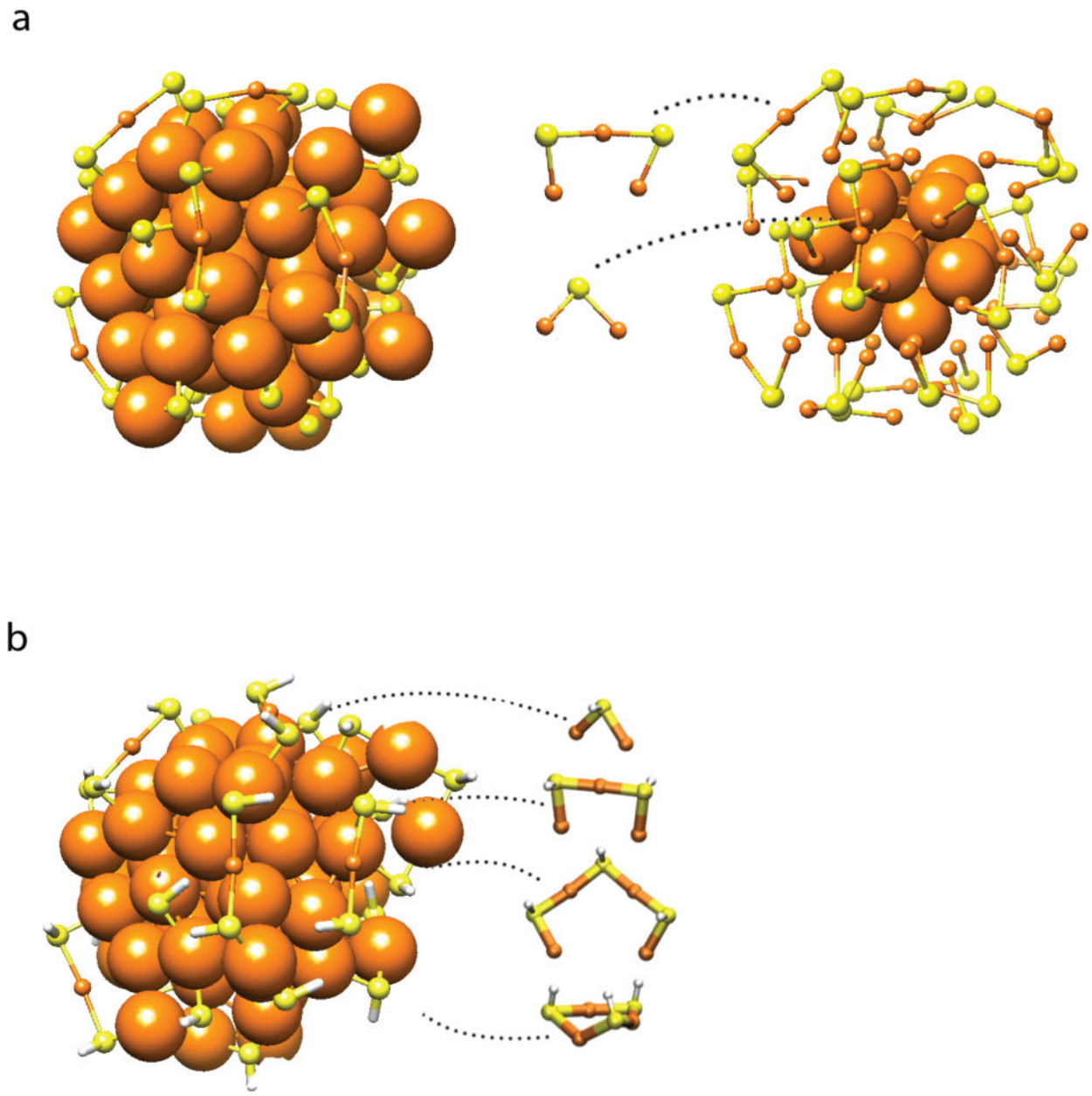

Figure 3. $Au_{68}(SH)_{32}$ model

(a) Addition of sulfur atoms (yellow) to gold framework (orange). Left, complete structure. Right, gold atoms outside the Au_{15} fcc core atoms depicted as small spheres to better reveal Au-S motifs. (b) Structure of $Au_{68}(SH)_{32}$ relaxed by DFT from the atomic positions from EM. Various gold-thiolate motifs (bridging thiolates, short and long staples, and a ring-like structure) are observed. Hydrogen atoms are white.

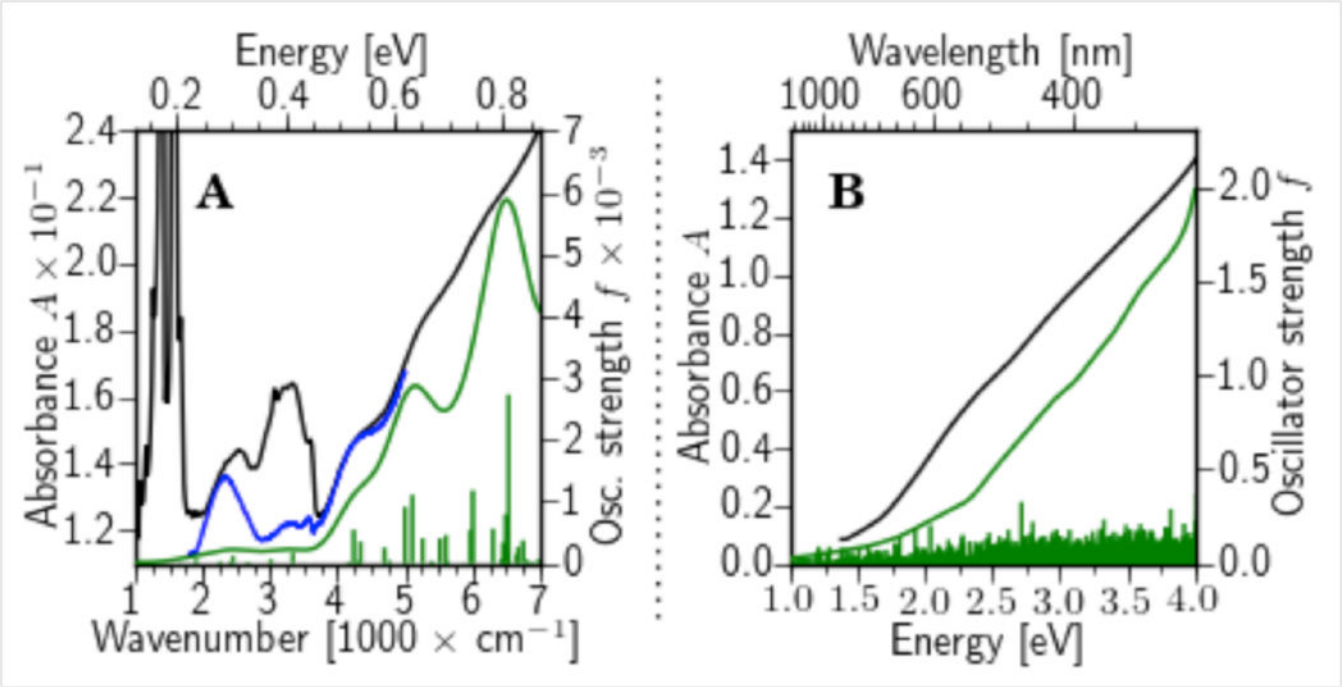

Figure 4. Measured and computed absorption spectra of the Au_{68}NP

(a) IR region, (b) UV-vis region. Black curves, experimental data. Green curves, LR-TDDFT computed spectra obtained from the individual optical transitions (green vertical sticks) with a Gaussian smoothing function (width 0.09 eV in (a) and 0.25 eV in (b)). Blue curve denotes a spectrum from which the vibrational contribution has been subtracted by reference to a spectrum of a larger cluster with the same ligand layer (see Fig. S10 for details). Both computed and the experimental data indicate that the lowest electronic transition occurs at 2500 cm^{-1} (0.31 eV).